

**Dynamic Nuclear Spin Polarization Induced by the Edelstein Effect at Bi(111) Surfaces**Zijian Jiang, V. Soghomonian, and J. J. Heremans<sup>\*</sup>*Department of Physics, Virginia Tech, Blacksburg, Virginia 24061, USA* (Received 9 June 2019; revised 7 July 2020; accepted 11 August 2020; published 3 September 2020)

Nuclear spin polarization induced by hyperfine interaction and mainly the Edelstein effect due to strong spin-orbit interaction, is investigated by quantum transport in Bi(111) thin film samples. The Bi(111) films are deposited on mica by van der Waals epitaxial growth. The Bi(111) films show micrometer-sized triangular islands with 0.39 nm step height, corresponding to the Bi(111) bilayer height. At low temperatures a high current density is applied to generate a nonequilibrium carrier spin polarization by mainly the Edelstein effect at the Bi(111) surface, which then induces dynamic nuclear polarization by hyperfine interaction. Comparative quantum magnetotransport antilocalization measurements indicate a suppression of antilocalization by the in-plane Overhauser field from the nuclear polarization and allow a quantification of the Overhauser field. Hence nuclear polarization was both achieved and quantified by a purely electronic transport-based approach.

DOI: [10.1103/PhysRevLett.125.106802](https://doi.org/10.1103/PhysRevLett.125.106802)

Spatial inversion symmetry exists in the Bi bulk but is broken normal to the surface, leading to strong Rashba-like spin-orbit interaction (SOI) due to the asymmetry of the surface-confinement potential for the two-dimensional (2D) surface states supported at the Bi(111) surface [1–3]. The Rashba parameter can reach  $\approx 0.5$  eV Å, substantially larger than in, e.g., InSb heterostructures [4,5]. Bi thin films further show a high carrier mobility and a long mean free path [6]. The Bi (111) surface states have therefore been of recent interest [7,8]. The Edelstein effect generates a nonequilibrium carrier spin polarization (CP) in materials with SOI in response to an applied electric field or a current density  $\mathbf{j}$ , with the spin polarization direction normal to  $\mathbf{j}$  and the surface normal [9–12]. The Edelstein effect has its origin in spin-momentum locking due to SOI. The effect can be pronounced at surfaces and interfaces with strong SOI, such as the Ag/Bi(111) [13,14] and Cu/Bi(111) [15] interfaces. Given the strong SOI at the Bi(111) surface, an in-plane  $\mathbf{j}$  in a Bi thin film is expected to generate a nonequilibrium in-plane CP. As explained in Ref. [16], here the Edelstein effect appears as the main contributor to the CP, likely augmented by contributions from the Bi spin Hall effect [13,14]. Hyperfine interaction (HI) can by dynamic nuclear polarization (DNP) transfer the CP to a nonequilibrium in-plane nuclear spin polarization (NP). The present work shows such CP-induced DNP, an example of the interplay between strong SOI, HI, and the Edelstein effect. The work also demonstrates that the effect of NP on quantum-coherent transport allows for a quantification of the polarization. The work is reminiscent of recent experiments where CP from the Edelstein effect generates a spin-transfer torque on magnetic moments [30], compared to this work where HI effectively mediates a spin-transfer torque on the nuclear spins. DNP from CP resulting from spin injection was

previously predicted [31] and the interplay between NP and CP from spin injection, mediated by HI, was studied in Fe/GaAs [17]. Another study used Faraday rotation to study DNP from current-induced NP in InGaAs [18]. The present experiments however differ from the latter [18] by using quantum magnetotransport measurements to quantify the DNP in an all-electrical setup, and by showing that the relatively higher carrier density in the Bi(111) surface states compared to semiconductors [17–20] allows DNP without application of an external magnetic field, relying only on the effective electronic field created by CP.

HI refers to the coupling of carrier spins to the nuclear spins by an energy term  $A\mathbf{I} \cdot \mathbf{J}$ , where  $A$  represents the hyperfine coupling constant [21,22],  $\mathbf{I}$  the nuclear spin, and  $\mathbf{J}$  the total carrier angular momentum. Two mechanisms contribute to HI [22,32,33], Fermi contact interaction (dominant when carrier and nuclear orbitals overlap [34]) and dipolar interaction [22,32]. HI can be more pronounced for heavy atoms featuring atomic parameters with higher energy scales [21,33], and for nuclei with large  $I$ . Both effects play a role strengthening HI for Bi, with  $I = 9/2$ . Further, electrons in Bi have a substantial  $s$ -orbital component at the Fermi energy,  $\sim 10\%$ , increasing the contact term and HI. The strong SOI in Bi may also enhance HI. Quantitative information on the strength of HI in semimetallic Bi is lacking. Yet experiments have studied the interaction between Bi donors in Si and the Si  $s$ -like conduction band carriers [23,24,33], concluding  $A = 6.1$   $\mu\text{eV}$ . The Knight shift in Bi<sub>2</sub>Se<sub>3</sub> shows  $A = 27$   $\mu\text{eV}$  [21]. Such values for  $A$  indicate that consequential HI is expected in semimetallic Bi as well as in Bi compounds. HI can lead to DNP where spin polarization is transferred from the carriers to the nuclei [35,36] and CP then generates NP. With NP established, the carriers

experience HI as an effective in-plane magnetic field having the same effect as an external Zeeman field, the Overhauser field  $B_{\text{OH}}$  [16,22,36,37]. Similarly, via HI the electronic CP results in an in-plane effective magnetic field  $B_e$  experienced by the nuclei [16,20]. For DNP to occur, the dipole-dipole interaction field  $B_L$  between neighboring nuclei ( $B_L \approx 0.024$  mT [16]) needs to be overcome by a nuclear Zeeman energy preventing a rapid  $T_2$  relaxation of NP [16,17,19,20].  $B_L$  can be overcome by a sufficiently large  $B_e$  [20]. In semiconductor experiments  $B_e$  is low due to the low carrier density, and overcoming the decay of NP then requires an external magnetic field  $> B_L$  [17–20]. In contrast, the present work shows that the higher carrier density in the Bi(111) surface states provides a  $B_e \gg B_L$  so that DNP can occur without an in-plane external magnetic field, and in fact application of an in-plane field keeps results unchanged [16].

$B_{\text{OH}}$  and the NP are here quantified by the antilocalization (AL) quantum coherence corrections to the conductance of the Bi(111) surface states, caused by quantum interference between backscattered time-reversed carrier trajectories under SOI. At low temperatures  $T$ , the AL corrections lead to a resistance  $R$  with a specific dependence on an external magnetic field  $B_{\perp}$  normal to the surface [25,38,39]. The magnetoresistance [MR,  $R(B_{\perp})$ ] due to AL is determined by three characteristic times [38,39]: the elastic scattering time  $\tau_0$  as deduced from the areal surface state density  $N_S$  and mobility  $\mu$ , the SOI spin decoherence time  $\tau_{\text{SO}}$ , and the quantum phase decoherence time  $\tau_{\phi}$ . Here  $\tau_{\text{SO}}^{-1} \propto \Delta_{\text{SO}}^2$  where  $\Delta_{\text{SO}}$  denotes the SOI splitting at the Fermi wave vector. The times are experimentally determined by quantitative fitting of the MR data to the AL theory developed by Iordanskii, Lyanda-Geller, and Pikus (ILP) [26] appropriate for the Bi(111) 2D surface states with Rashba-like SOI [16]. The influence of magnetization on AL in ferromagnetic materials has been theoretically studied [40]. We expect similar effects due to NP, supported by the theoretical treatment of  $B_{\text{OH}}$  as an effective in-plane magnetic field  $B_{\parallel}$  [41,42]. Specifically,  $B_{\parallel}$  generates an effective Zeeman splitting which aligns the carrier spins and hence suppresses the Cooperon in the spin singlet channel and thereby inhibits AL [40]. The inhibition of AL is visible in the data as an increase in  $\tau_{\text{SO}}$  with increasing  $B_{\parallel}$ . Further, AL is a sensitive probe of quantum and spin coherence [38], and is sensitive to the time-reversal symmetry (TRS) breaking due to  $B_{\parallel}$  [40,43,44]. The breaking of TRS due to the interplay of Zeeman splitting and SOI results in a quantifiable decrease in  $\tau_{\phi}$  [43] with increasing  $B_{\parallel}$ , also visible in the data. Identifying  $B_{\parallel} = B_{\text{OH}}$ , we thus use AL as a sensitive probe of DNP and HI which allows a quantification of  $B_{\text{OH}}$ .

An optimized van der Waals epitaxy (vdWE) [27] was used to grow the Bi(111) films on mica substrates, resulting in large grain sizes with the trigonal axis perpendicular to the film plane [16]. vdWE is particularly suited to the

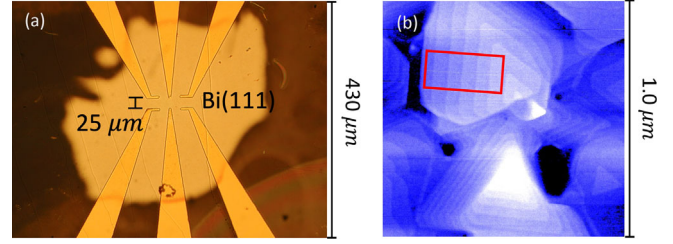


FIG. 1. (a) Optical micrograph of the 40 nm thick Bi film sample grown on mica by van der Waals epitaxy, with lithographic Au contacts. The diameter of the sample is  $\sim 350 \mu\text{m}$ ; distance between contacts  $\sim 25 \mu\text{m}$ . (b) AFM micrograph of a  $1 \mu\text{m} \times 1 \mu\text{m}$  region of the Bi film clearly illustrates layered growth. Step analysis in the red boxed region indicates a step height of  $0.391 \pm 0.015$  nm, as expected for  $1.0 \text{ BL}_{111}$ .

unstrained growth of weakly bonding materials such as Bi [28,29]. The 40 nm thick Bi(111) was deposited through a shadowmask, yielding samples of diameter  $\sim 350 \mu\text{m}$ . Au contacts were photolithographically patterned after film deposition [Fig. 1(a)]. Atomic force microscopy indicated a layered step surface with triangular terraces [Fig. 1(b)] and showed a step height between adjacent terraces of  $0.391 \pm 0.015$  nm, corresponding to one Bi(111) bilayer height ( $\text{BL}_{111} = 0.39$  nm) [16].

The AL and transport coefficient characterization were carried out by magnetotransport in a  $^3\text{He}$  immersion cryostat down to  $T = 0.39$  K, using standard 4-contact ac lock-in techniques with current of  $2 \mu\text{A}$  rms under applied  $B_{\perp}$ . To develop DNP a high dc polarization current,  $I_p = 0.5$  mA to 1.5 mA,  $\mathbf{j} \sim 6.25 \times 10^7$  A/m $^2$  to  $1.9 \times 10^8$  A/m $^2$ , was applied at  $T = 0.39$  K between a pair of contacts for variable polarization durations  $t_p$  from 10 to 120 min.  $I_p$  was removed after the DNP step, letting the NP and  $B_{\text{OH}}$  decay slowly with a spin-lattice relaxation time  $T_1$  characteristic of the nuclear decoherence [45,46]. The slow decay allowed time for the subsequent observation of DNP from AL measurements. For AL measurements the voltage was measured over the same contacts to which  $I_p$  was applied and hence over the path of which  $B_{\text{OH}}$  develops, as depicted in Fig. 2. For the AL data it is sufficient to sweep  $B_{\perp}$  over  $\sim 0.2$  T, achievable in as little as  $\sim 15$  min, of the order of the expected  $T_1$  [47,48]. Experiments were also performed with different delay times  $t_{\text{delay}}$ , from 15 to 40 min, inserted between removing  $I_p$  and performing the AL measurement, to characterize the decay in  $B_{\text{OH}}$  and estimate  $T_1$ .

$N_S$  and  $\mu$  were determined from magnetotransport at 0.39 K, indicating predominantly  $n$ -type surface carrier contribution. We determine  $N_S = 1.95 \times 10^{15} \text{ m}^{-2}$ ,  $\mu = 1.00 \text{ m}^2/\text{Vs}$ ,  $\tau_0 = 0.0856$  ps and mean free path  $l_0 = v_f \tau_0 = 20.4$  nm, where  $v_f$  is the Fermi velocity derived from  $N_S$ . As appropriate for surface states we use the 2D diffusion constant  $D$  calculated as  $D = \frac{1}{2} v_f^2 \tau_0$ , at  $T = 0.39$  K yielding  $D = 0.00243 \text{ m}^2/\text{s}$ . AL results in a

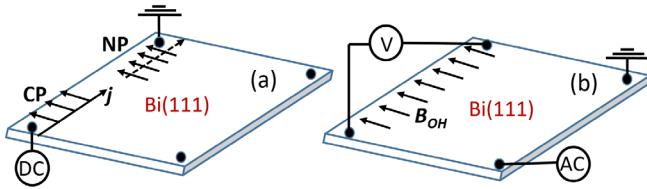


FIG. 2. Schematic of the Edelstein-induced DNP and AL setup for Bi(111) surface states. (a) A high dc current density  $\mathbf{j}$  in the Bi film sample induces a nonequilibrium carrier spin polarization by mainly the Edelstein effect. The surface-state carrier spins are oriented perpendicular to  $\mathbf{j}$ , and induce an in-plane surface nuclear spin polarization via DNP, resulting in in-plane Overhauser field  $B_{OH}$ . (b) After  $\mathbf{j}$  is removed and while  $B_{OH}$  slowly decays, AL measurements are carried out.

characteristic positive quantum correction in  $R(B_{\perp})$  at  $B_{\perp} \lesssim 0.04$  T, expressed as a small correction to the 2D conductivity  $\sigma_2(B)$ . We define  $\Delta\sigma_2(B_{\perp}) = \sigma_2(B_{\perp}) - \sigma_2(B_{\perp} = 0)$  and  $\Delta R(B_{\perp}) = R(B_{\perp}) - R_0$  where  $R_0 = R(B_{\perp} = 0)$ . Since  $\Delta R(B_{\perp}) \ll R_0$ , we have  $\Delta\sigma_2(B_{\perp})/\sigma_2(B_{\perp} = 0) \approx -\Delta R(B_{\perp})/R_0$ , allowing fits to  $\Delta\sigma_2(B_{\perp})$  from the experimental MR. To fit the data the ILP theory [26] is applied, including only the Rashba SOI term (details in Ref. [16]). Since  $\tau_0$  merely produces a shift in  $\Delta\sigma_2(B_{\perp})$ ,  $\tau_{\phi}$  and  $\tau_{SO}$  are the only two free fitting parameters. The fits are performed for AL obtained after different  $t_p$  and  $t_{delay}$  under different  $I_p$ . From the fits, we find the dependences on  $t_p$ ,  $t_{delay}$  and  $I_p$  of  $\tau_{SO}$  and  $\tau_{\phi}$ . From the latter the dependences of  $B_{OH}$  are determined.

Figure 3 depicts representative MR of the Bi film sample at  $T = 0.39$  K before and after DNP using variable  $I_p$  ranging from 0.5 mA to 1.5 mA and  $t_p$  ranging from 0 (before DNP) to 120 min (at  $t_{delay} = 0$ ). The positive MR characteristic of AL is observed both before and after DNP. The negative of  $\Delta\sigma_2(B_{\perp})$  [reproducing  $\Delta R(B_{\perp})$ ] at low  $B_{\perp}$

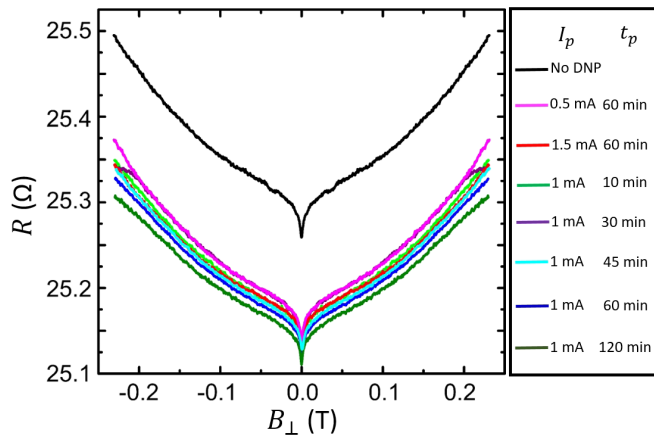


FIG. 3. AL magnetoresistance at  $T = 0.39$  K before (indicated as No DNP) and after DNP with variable  $I_p$  and variable  $t_p$  ( $t_{delay} = 0$ ; traces not offset). After DNP a widening of  $R(B_{\perp})$  vs  $B_{\perp}$  for  $B_{\perp} \neq 0$  is evident.

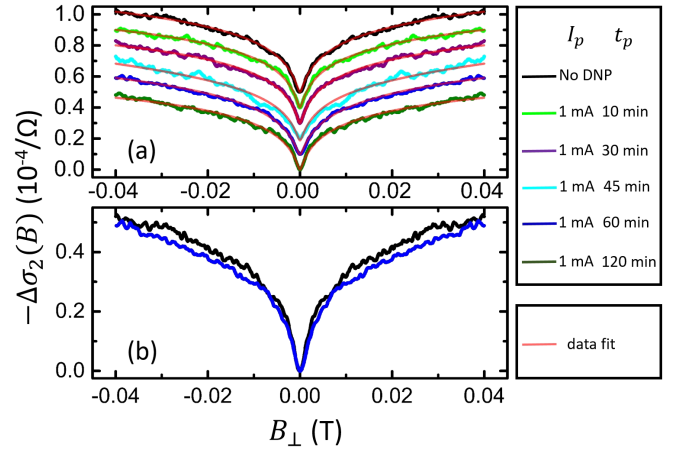


FIG. 4. 2D conductivity corrections due to AL at  $T = 0.39$  K and at low  $B_{\perp}$  ( $t_{delay} = 0$ ): (a) under variable  $t_p$  with  $I_p = 1$  mA. The red traces indicate fits to the AL theory [26]. Data are offset for clarity; (b) before DNP (black trace) and after DNP (blue trace) with  $t_p = 60$  min and  $I_p = 1$  mA (traces not offset). The widening of the trace after DNP indicates a partial suppression of AL by  $B_{OH}$ .

is displayed in Fig. 4(a) for variable  $t_p$  when  $I_p = 1$  mA (at  $t_{delay} = 0$ ). Best fits to the ILP theory [16,26] overlay the data in Fig. 4(a) in red and indicate that the theory excellently captures the AL in the Bi(111) surface states and will allow reliable extraction of values for  $\tau_{SO}$  and  $\tau_{\phi}$ . The traces for  $R(B_{\perp})$  (Fig. 3) and for  $-\Delta\sigma_2(B_{\perp})$  [Fig. 4(a)] show a widening vs  $B_{\perp}$  for  $B_{\perp} \neq 0$  after DNP, characteristic of an increase in  $\tau_{SO}$  (decreasing effect of SOI) and a decrease in  $\tau_{\phi}$  as confirmed below. The widening shows a dependence on  $I_p$  and  $t_p$ , with long  $t_p = 120$  min at  $I_p = 1$  mA resulting in the largest effect. The dependence on  $t_p$  and  $I_p$  suggests DNP and hence  $B_{OH}$  play a role in changing  $\tau_{SO}$  and  $\tau_{\phi}$ . The widening of the minimum in  $-\Delta\sigma_2(B_{\perp})$  is further illustrated in Fig. 4(b) where the black trace represents  $-\Delta\sigma_2(B_{\perp})$  before DNP and the blue trace after DNP with  $t_p = 60$  min and  $I_p = 1$  mA (at  $t_{delay} = 0$ ). Before we present quantitative data on  $\tau_{SO}$  and  $\tau_{\phi}$ , we note that the AL results after DNP are qualitatively consistent with the existence of in-plane  $B_{OH}$ . Phenomenologically, after removing  $I_p$ ,  $B_{OH}$  persists and generates an effective Zeeman energy  $g_{\parallel}^* \mu_B B_{OH}$ , where  $g_{\parallel}^*$  denotes the in-plane  $g$  factor (for Bi(111) surface states,  $g_{\parallel}^* \approx 33$  [8]) and  $\mu_B$  denotes the Bohr magneton.  $B_{OH}$  partially aligns the carrier spins and suppresses the spin phase shift due to SOI and thereby weakens AL [40,43,49]. The effect leads to a widening of the characteristic sharp minimum in  $\Delta R(B_{\perp})$  vs  $B_{\perp}$  and is quantified by a lengthening of  $\tau_{SO}$ . Further,  $B_{OH}$  results in a spin-induced TRS breaking [42,43,49], leading to a decrease in  $\tau_{\phi}$ . While it is not in the scope of this experimental study to modify the ILP theory to include HI, future theoretical studies

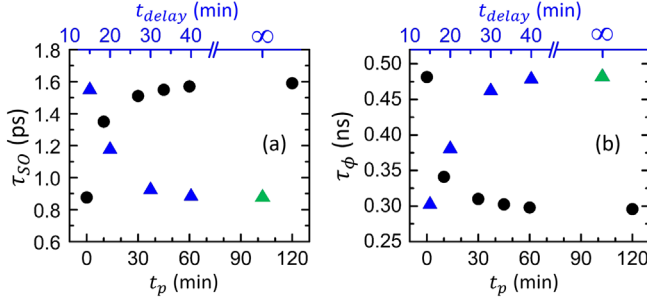


FIG. 5. (a) Spin-orbit decoherence times  $\tau_{SO}$  and (b) quantum phase decoherence times  $\tau_\phi$  at  $T = 0.39$  K and  $I_p = 1$  mA, vs DNP duration  $t_p$  ( $t_{delay} = 0$ ) (black circles) and vs  $t_{delay}$  ( $t_p = 60$  min) (blue triangles). Data without DNP stand in for  $t_p = 0$  and for  $t_{delay} \rightarrow \infty$  (green triangles).

specific to the influence of HI and NP on AL may help refine quantitative aspects of the experiments, as was performed for ferromagnetic order [40] and for Zeeman interaction [42].

The dependences of  $\tau_{SO}$  and  $\tau_\phi$  on  $t_p$  at fixed  $I_p = 1$  mA with  $t_{delay} = 0$  are presented in Figs. 5(a) and 5(b). The value of  $\tau_{SO}$  increases with increasing  $t_p$  [Fig. 5(a)], indicative of the influence of the in-plane  $B_{OH}$ . A phenomenological understanding was presented above. Theoretical studies of the combined influence of SOI and  $B_{\parallel}$  on an inhomogeneous interfacial spin distribution [50] show that even a weak  $B_{\parallel}$  results in a decrease of the spin density proportional to  $1/(2\pi D\tau_{SO})$ , relating an increase in  $\tau_{SO}$  to the influence of  $B_{\parallel} = B_{OH}$ . Figure 5(b) shows a decrease of  $\tau_\phi$  with increasing  $t_p$ , and similar to Fig. 5(a) manifests a saturation at higher  $t_p$ . The decrease of  $\tau_\phi$  with increasing  $t_p$  is indicative of the interplay of the effective Zeeman energy and SOI [42,43], predicted to result in a quadratic dependence of  $\tau_\phi$  on  $B_{\parallel}$  [43]:

$$\frac{\tau_\phi(B_{\parallel})}{\tau_\phi(B_{\parallel} = 0)} = \frac{1}{1 + cB_{\parallel}^2}, \quad (1)$$

where  $c = \tau_\phi(B_{\parallel} = 0)\tau_{SO}(B_{\parallel} = 0)(g_{\parallel}^*\mu_B/\hbar)^2$ . The estimated average value of  $B_{OH} = B_{\parallel}$  can be calculated from the data using Eq. (1). Figures 5(a) and 5(b) depict the dependences of  $\tau_{SO}$  and  $\tau_\phi$  on  $t_{delay}$  at  $I_p = 1$  mA and  $t_p = 60$  min ( $-\Delta\sigma_2(B_{\perp})$  in Ref. [16]). With increasing  $t_{delay}$ ,  $\tau_{SO}$  decreases and  $\tau_\phi$  increases to their values without DNP, consistent with a decay in  $B_{OH}$ . Figure 6 shows the average  $B_{OH}$  calculated from  $\tau_\phi$  in Fig. 5(b). Since the AL measurement (sweeping over  $B_{\perp} \sim 0.2$  T after removing  $I_p$  and waiting  $t_{delay}$ ) spans  $\sim 15$  min, by estimated average  $B_{OH}$  is meant the value after averaging over these  $\sim 15$  min. Current spreading between the current contacts over the sample geometry during DNP will likely lead to nonuniform DNP, and  $B_{OH}$  hence encompasses spatial averaging

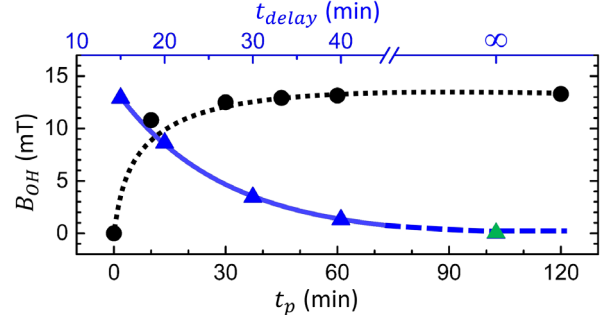


FIG. 6. Overhauser field  $B_{OH}$  at  $T = 0.39$  K and  $I_p = 1$  mA, vs DNP duration  $t_p$  ( $t_{delay} = 0$ ) (black circles) and vs  $t_{delay}$  ( $t_p = 60$  min) (blue triangles). Data without DNP stand in for  $t_p = 0$  and for  $t_{delay} \rightarrow \infty$  (green triangle). The black dotted line is a guide to the eye. The blue line is an exponential fit yielding  $T_1 = 11.4$  min.

as well. To minimize handling of the data, the averaging effects are not accounted for in Fig. 6 but should be kept in mind. In Fig. 6 the average  $B_{OH}$  increases with increasing  $t_p$ , and saturates at about 13 mT. An exponential fit showed that the increase towards saturation occurs with a characteristic time  $T_1 e = 6 \dots 11$  min, with  $T_1 e$  characterizing the expected nuclear spin alignment by DNP [20]. In Fig. 6, the average  $B_{OH}$  decays exponentially with increasing  $t_{delay}$ , with spin-lattice relaxation time  $T_1 = 11.4$  min. The value  $T_1 = 11.4$  min is of the order of expected values [47,48].  $B_{OH}$  depends on the average nuclear spin  $I_{av}$  after NP, as  $B_{OH} = AI_{av}/(g_{\parallel}^*\mu_B)$  [16,20,51], and  $I_{av}$  follows a Brillouin function in the average carrier spin  $S_{av}$  after CP [16,20]. Using values of  $A = 6.1 \mu\text{eV}$  to  $27 \mu\text{eV}$  [21,23,24,33] we find that  $B_{OH} = 13$  mT is reached for  $S_{av} = 0.37$  if  $A = 6.1 \mu\text{eV}$  and for  $S_{av} = 0.20$  if  $A = 27 \mu\text{eV}$  [16]. Since we do not expect full NP ( $S_{av} = \frac{1}{2}$ ) and  $B_{OH}$  involves averages described above, the saturation value of 13 mT is consistent with the knowledge of  $A$  in Bi and with plausible values of  $S_{av}$ . For  $B_{OH} = 13$  mT and in this range of  $A$  it is calculated that  $B_e \gg B_L$ , consistent with the observation of DNP without external magnetic field [16]. Also, the dependence of  $B_{OH}$  on  $I_p$  strongly resembles the expected Brillouin function [16], strengthening the consistency between expectations and data. The saturation value  $B_{OH} = 13$  mT and the dependences on  $t_p$ ,  $t_{delay}$  and  $I_p$  firmly suggest that the CP due mainly to the Edelstein effect was transferred by HI to the Bi nuclei, demonstrating Edelstein-induced DNP and its measurement by quantum transport.

In conclusion, Bi(111) thin films were deposited by van der Waals epitaxy on mica substrates. Using antilocalization quantum-coherent transport measurements on the Bi (111) surface states to detect in-plane magnetic fields, quantitative evidence was obtained for a transfer of carrier spin polarization to Bi nuclear spin polarization by hyperfine interaction. The carrier spin polarization was obtained via mainly the Edelstein effect in the Bi(111) surface states.

The experiments verify the existence of Edelstein-induced dynamic nuclear polarization, in an example of interaction between spin-orbit interaction and hyperfine interaction via the nuclear spin bath, with possible applications in nuclear spintronics and to polarize nuclei to mitigate spin decoherence via HI in quantum devices. The experiments also show that antilocalization forms a sensitive probe for hyperfine interaction and nuclear polarization.

The work was supported by the U.S. Department of Energy, Office of Basic Energy Sciences, Division of Materials Sciences and Engineering under Award No. DOE DE-FG02-08ER46532.

\*Corresponding author.  
heremans@vt.edu

- [1] Yu. M. Koroteev, G. Bihlmayer, J. E. Gayone, E. V. Chulkov, S. Blügel, P. M. Echenique, and Ph. Hofmann, *Phys. Rev. Lett.* **93**, 046403 (2004).
- [2] Ph. Hofmann, *Prog. Surf. Sci.* **81**, 191 (2006).
- [3] T. Hirahara, K. Miyamoto, I. Matsuda, T. Kadono, A. Kimura, T. Nagao, G. Bihlmayer, E. V. Chulkov, S. Qiao, K. Shimada, H. Namatame, M. Taniguchi, and S. Hasegawa, *Phys. Rev. B* **76**, 153305 (2007).
- [4] M. Rudolph and J. J. Heremans, *Phys. Rev. B* **83**, 205410 (2011).
- [5] R. L. Kallaher, J. J. Heremans, N. Goel, S. J. Chung, and M. B. Santos, *Phys. Rev. B* **81**, 075303 (2010).
- [6] Z. Zhu, B. Fauqué, Y. Fuseya, and K. Behnia, *Phys. Rev. B* **84**, 115137 (2011).
- [7] B. E. Feldman, M. T. Randeria, A. Gyenis, F. Wu, H. Ji, R. J. Cava, A. H. MacDonald, and A. Yazdani, *Science* **354**, 316 (2016).
- [8] H. Du, X. Sun, X. Liu, X. Wu, J. Wang, M. Tian, A. Zhao, Y. Luo, J. Yang, B. Wang, and J. G. Hou, *Nat. Commun.* **7**, 10814 (2016).
- [9] V. M. Edelstein, *Solid State Commun.* **73**, 233 (1990).
- [10] J. Borge, C. Gorini, G. Vignale, and R. Raimondi, *Phys. Rev. B* **89**, 245443 (2014).
- [11] K. Shen, G. Vignale, and R. Raimondi, *Phys. Rev. Lett.* **112**, 096601 (2014).
- [12] D. Pesin and A. H. MacDonald, *Nat. Mater.* **11**, 409 (2012).
- [13] J. C. R. Sánchez, L. Vila, G. Desfonds, S. Gambarelli, J. P. Attané, J. M. De Teresa, C. Magén, and A. Fert, *Nat. Commun.* **4**, 2944 (2013).
- [14] S. Sangiao, J. M. De Teresa, L. Morellon, I. Lucas, M. C. Martínez-Velarte, and M. Viret, *Appl. Phys. Lett.* **106**, 172403 (2015).
- [15] M. Isasa, M. C. Martínez-Velarte, E. Villamor, C. Magén, L. Morellón, J. M. De Teresa, M. R. Ibarra, G. Vignale, E. V. Chulkov, E. E. Krasovskii, L. E. Hueso, and F. Casanova, *Phys. Rev. B* **93**, 014420 (2016).
- [16] See Supplemental Material at <http://link.aps.org/supplemental/10.1103/PhysRevLett.125.106802> for growth, Edelstein effect, fitting,  $B_{OH}$ ,  $B_e$ , dependence on  $I_p$  and data, including Refs. [2–5,8,13–15,17–29].
- [17] G. Salis, A. Fuhrer, and S. F. Alvarado, *Phys. Rev. B* **80**, 115332 (2009).
- [18] C. J. Trowbridge, B. M. Norman, Y. K. Kato, D. D. Awschalom, and V. Sih, *Phys. Rev. B* **90**, 085122 (2014).
- [19] D. Paget, G. Lampel, B. Sapoval, and V. I. Safarov, *Phys. Rev. B* **15**, 5780 (1977).
- [20] F. Meier and B. P. Zakharchenya, *Optical Orientation* (North Holland, 1984), Chap. 2 & 5.
- [21] D. M. Nisson, A. P. Dioguardi, P. Klavins, C. H. Lin, K. Shirer, A. C. Shockley, J. Crocker, and N. J. Curro, *Phys. Rev. B* **87**, 195202 (2013).
- [22] I. Tifrea and M. E. Flatté, *Phys. Rev. B* **84**, 155319 (2011).
- [23] R. E. George, W. Witzel, H. Riemann, N. V. Abrosimov, N. Nötzel, M. L. W. Thewalt, and J. J. L. Morton, *Phys. Rev. Lett.* **105**, 067601 (2010).
- [24] G. W. Morley, M. Warner, A. M. Stoneham, P. T. Greenland, J. van Tol, C. W. M. Kay, and G. Aeppli, *Nat. Mater.* **9**, 725 (2010).
- [25] L. E. Golub, *Phys. Rev. B* **71**, 235310 (2005).
- [26] S. V. Iordanskii, Yu. B. Lyanda-Geller, and G. E. Pikus, *JETP Lett.* **60**, 206 (1994).
- [27] A. Koma, *J. Cryst. Growth* **201–202**, 236 (1999).
- [28] H. J. Osten, J. Klatt, and G. Lippert, *Appl. Phys. Lett.* **60**, 44 (1992).
- [29] A. J. Littlejohn, Y. Xiang, E. Rauch, T.-M. Lu, and G.-C. Wang, *J. Appl. Phys.* **122**, 185305 (2017).
- [30] S. Emori, T. Nan, A. M. Belkessam, X. Wang, A. D. Matyushov, C. J. Babroski, Y. Gao, H. Lin, and N. X. Sun, *Phys. Rev. B* **93**, 180402(R) (2016).
- [31] M. Johnson, *Appl. Phys. Lett.* **77**, 1680 (2000).
- [32] S. Mukhopadhyay, S. Krämer, H. Mayaffre, H. F. Legg, M. Orlita, C. Berthier, M. Horvatić, G. Martínez, M. Potemski, B. A. Piot, A. Materna, G. Strzelecka, and A. Hruban, *Phys. Rev. B* **91**, 081105(R) (2015).
- [33] G. Feher, *Phys. Rev.* **114**, 1219 (1959).
- [34] M. Bucher, *Eur. J. Phys.* **21**, 19 (2000).
- [35] G. Sharma, T. Gaebel, E. Rej, D. J. Reilly, S. E. Economou, and E. Barnes, *Phys. Rev. B* **99**, 205423 (2019).
- [36] A. Del Maestro, T. Hyart, and B. Rosenow, *Phys. Rev. B* **87**, 165440 (2013).
- [37] V. Tripathi, A. C. H. Cheung, and N. R. Cooper, *Europhys. Lett.* **81**, 68001 (2008).
- [38] V. Deo, Y. Zhang, V. Soghomonian, and J. J. Heremans, *Sci. Rep.* **5**, 9487 (2015); Y. Zhang, V. Soghomonian, and J. J. Heremans, *Phys. Rev. B* **97**, 155439 (2018).
- [39] G. Bergmann, *Phys. Rep.* **107**, 1 (1984); *Int. J. Mod. Phys. B* **24**, 2015 (2010).
- [40] V. K. Dugaev, P. Bruno, and J. Barnaś, *Phys. Rev. B* **64**, 144423 (2001).
- [41] Yu. F. Komnik, V. V. Andrievskii, and I. B. Berkutov, *Low Temp. Phys.* **33**, 79 (2007).
- [42] A. G. Mal'shukov, K. A. Chao, and M. Willander, *Phys. Rev. B* **56**, 6436 (1997).
- [43] F. E. Meijer, A. F. Morpurgo, T. M. Klapwijk, T. Koga, and J. Nitta, *Phys. Rev. B* **70**, 201307(R) (2004).
- [44] B. L. Al'tshuler and A. G. Aronov, *JETP Lett.* **33**, 499 (1981).
- [45] G. Yusa, K. Muraki, K. Takashina, K. Hashimoto, and Y. Hirayama, *Nature (London)* **434**, 1001 (2005).
- [46] Z. K. Keane, M. C. Godfrey, J. C. H. Chen, S. Fricke, O. Klochan, A. M. Burke, A. P. Micolich, H. E. Beere,

- D. A. Ritchie, K. V. Trunov, D. Reuter, A. D. Wieck, and A. R. Hamilton, *Nano Lett.* **11**, 3147 (2011).
- [47] G. Lampel, *Phys. Rev. Lett.* **20**, 491 (1968).
- [48] W. Heil, H. Humblot, E. Otten, M. Schafer, R. Sarkau, and M. Leduc, *Phys. Lett. A* **201**, 337 (1995).
- [49] F. E. Meijer, A. F. Morpurgo, T. M. Klapwijk, and J. Nitta, *Phys. Rev. Lett.* **94**, 186805 (2005).
- [50] V. A. Frolov, *Phys. Rev. B* **64**, 045311 (2001).
- [51] S. Tenberg, R. P. G. McNeil, S. Rubbert, and H. Bluhm, *Phys. Rev. B* **92**, 195428 (2015).